# Neural networks with physical constraints, domain decomposition-based training strategies, and model order reduction

Alexander Heinlein

BOOTCAMP: NVIDIA/HLRS SciML GPU Bootcamp, Online, October 24, 2022

Delft University of Technology

# Scientific Machine Learning in Computational Science and Engineering

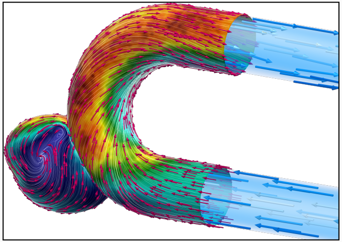 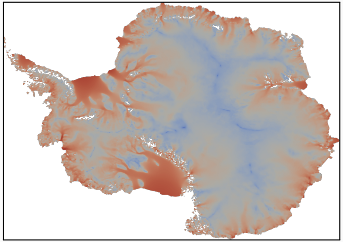 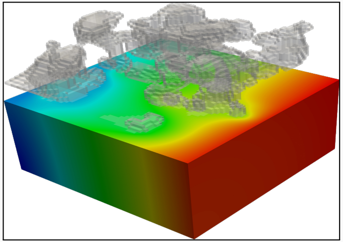

## Numerical methods

**Based on physical models**

+ Robust and generalizable
− Require availability of mathematical models

## Machine learning models

**Driven by data**

+ Do not require mathematical models
− Sensitive to data, limited extrapolation capabilities

## Scientific machine learning (SciML)

**Combining the strengths** and **compensating the weaknesses** of the individual approaches:

numerical methods **improve** machine learning techniques
machine learning techniques **assist** numerical methods

# Scientific Machine Learning as a Standalone Field


N. Baker, A. Frank, T. Bremer, A. Hagberg, Y. Kevrekidis, H. Najm, M. Parashar, A. Patra, J. Sethian, S. Wild, K. Willcox, and S. Lee. **Workshop Report on Basic Research Needs for Scientific Machine Learning: Core Technologies for Artificial Intelligence.** USDOE Office of Science (SC), Washington, DC (United States), 2019.

## Priority Research Directions

Foundational research themes:

- Domain-awareness
- Interpretability
- Robustness

Capability research themes:

- Massive scientific data analysis
- Machine learning-enhanced modeling and simulation
- Intelligent automation and decision-support for complex systems

# Development of the Field of Scientific Machine Learning

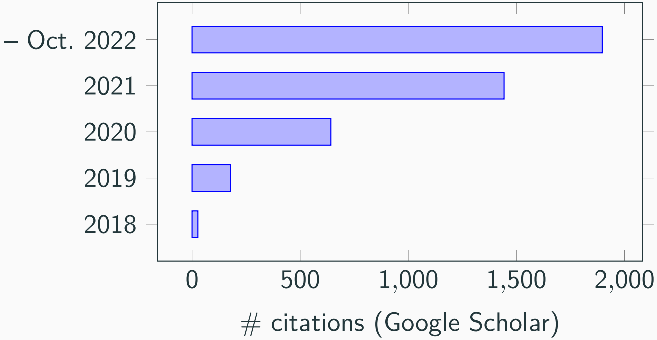


M. Raissi, P. Perdikaris, and G. E. Karniadakis.
**Physics-informed neural networks: A deep learning framework for solving forward and inverse problems involving nonlinear partial differential equations.**
Journal of Computational physics, 378, 686-707. 2019.

(and the respective arXiv preprints)

# Scientific Machine Learning Examples

Many approaches in scientific machine learning have been developed in the past few years.

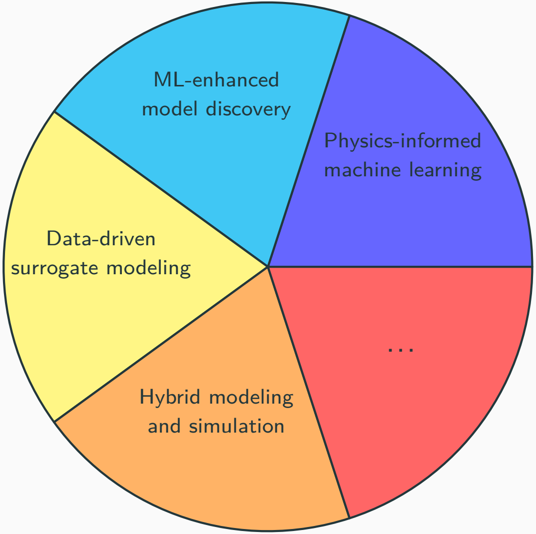

# Scientific Machine Learning Examples

Many approaches in scientific machine learning have been developed in the past few years. We will focus on **two types**:

**Data-driven surrogate modeling**

Replacing a **computationally expensive** numerical simulator by a **fast** data-driven model.

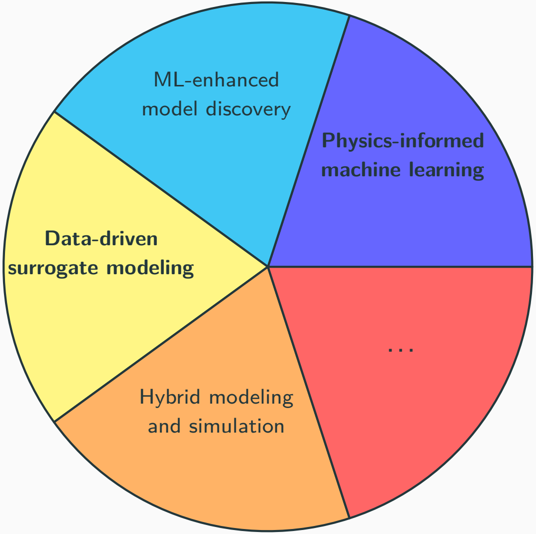


**Physics-informed machine learning**

**Regularizing** a data-driven machine learning model using a physics-based model.

# Outline

1. Physics-informed machine learning

2. Domain decomposition-based training strategies for PINNs

   Based on joint work with Victorita Dolean (University of Strathclyde), and Benjamin Moseley and Siddhartha Mishra (ETH Zürich)

3. Surrogate models for computational fluid dynamics simulations – Data-driven approach

   Based on joint work with Mattias Eichinger and Axel Klawonn (University of Cologne)

4. Surrogate models for computational fluid dynamics simulations – Physics-aware approach

   Based on joint work with Viktor Grimm, and Axel Klawonn (University of Cologne)

# Physics-informed machine learning

# Artificial Neural Networks for Solving Ordinary and Partial Differential Equations

Isaac Elias Lagaris, Aristidis Likas, *Member, IEEE*, and Dimitrios I. Fotiadis

**Published in IEEE TRANSACTIONS ON NEURAL NETWORKS, VOL. 9, NO. 5, 1998.**

**Idea:** Solve a general differential equation subject to boundary conditions

$$G(\mathbf{x}, \Psi(\mathbf{x}), \nabla\Psi(\mathbf{x}), \nabla^2\Psi(\mathbf{x})) = 0 \quad \text{in } \Omega$$

by solving an **optimization problem**

$$\min_{\mathbf{p}} \sum_{\mathbf{x}_i} G(\mathbf{x}_i, \Psi_t(\mathbf{x}_i, \mathbf{p}), \nabla\Psi_t(\mathbf{x}_i, \mathbf{p}), \nabla^2\Psi_t(\mathbf{x}_i), \mathbf{p})^2$$

where $\Psi_t(\mathbf{x}, \mathbf{p})$ is a **trial function**, $\mathbf{x}_i$ **sampling points inside the domain** $\Omega$ and $\mathbf{p}$ are **adjustable parameters**.

# Main Features of the Method

### Construction of the trial functions

The trial functions **explicitly satisfy the boundary conditions**:

$$\Psi_t(\mathbf{x}, \mathbf{p}) = A(\mathbf{x}) + F(\mathbf{x}, N(\mathbf{x}, \mathbf{p})),$$

where

- $N(\mathbf{x}, \mathbf{p})$ is a **trainable feedforward neural network** with parameters $\mathbf{p}$ and input $x \in \mathbb{R}^n$ and
- the functions $A$ and $F$ are **fixed functions** chosen such that
  - $A$ **satisfies the boundary conditions**, and
  - $F$ **does not contribute to the boundary conditions**.

From the conclusion of the paper:

> *"The **success of the method** can be attributed to **two factors**. The first is the employment of neural networks that are **excellent function approximators** and the second is the form of the **trial solution that satisfies by construction the BC's** and therefore the constrained optimization problem becomes a substantially simpler unconstrained one."*

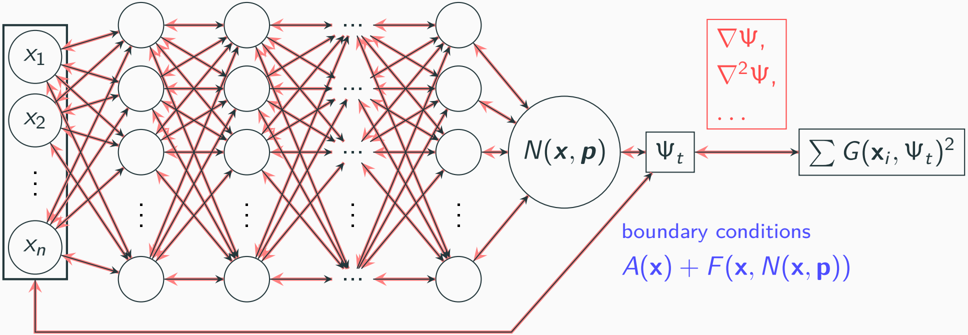

$x_1$
$x_2$
$x_n$
$N(\boldsymbol{x}, \boldsymbol{p})$
$\Psi_t$
$\nabla \Psi$,
$\nabla^2 \Psi$,
...
$\sum G(\mathbf{x}_i, \Psi_t)^2$
boundary conditions
$A(\mathbf{x}) + F(\mathbf{x}, N(\mathbf{x}, \mathbf{p}))$

# Physics-Informed Neural Networks (PINNs)

In **Raissi, Perdikaris, Karniadakis (2019)**, the authors have revisited and modified the approach by **Lagaris et al. (1998)**, denoting their method as **physics-informed neural networks (PINNs)**. Consider the partial differential equation

$$\mathcal{N}[u](\boldsymbol{x}, \boldsymbol{t}) \quad = \quad f(\boldsymbol{x}, \boldsymbol{t}), \qquad (\boldsymbol{x}, \boldsymbol{t}) \in [0, T] \times \Omega \subset \mathbb{R}^d.$$

The main novelty of PINNs is that a **hybrid loss function** is used for training the feedforward neural network:

$$\mathcal{L} = \omega_{\text{data}} \mathcal{L}_{\text{data}} + \omega_{\text{PDE}} \mathcal{L}_{\text{PDE}},$$

where $\omega_{\text{data}}$ and $\omega_{\text{PDE}}$ are **weights** and

$$\mathcal{L}_{\text{data}} \quad = \quad \frac{1}{N_{\text{data}}} \sum_{i=1}^{N_{\text{data}}} \left( u(x_i, t_i) - u_i \right)^2,$$

$$\mathcal{L}_{\text{PDE}} \quad = \quad \frac{1}{N_{\text{PDE}}} \sum_{i=1}^{N_{\text{data}}} \left( \mathcal{N}[u](\boldsymbol{x}, \boldsymbol{t}) - f(\boldsymbol{x}, \boldsymbol{t}) \right)^2.$$

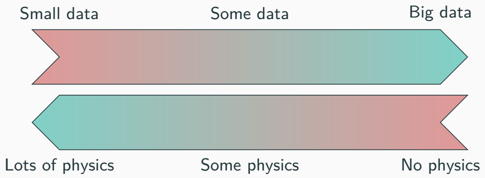


- **Known solution values** can be included in $\mathcal{L}_{\text{data}}$.
- **Initial and boundary conditions** are also included in $\mathcal{L}_{\text{data}}$

# Sketch of the PINN approach by Raissi et al.

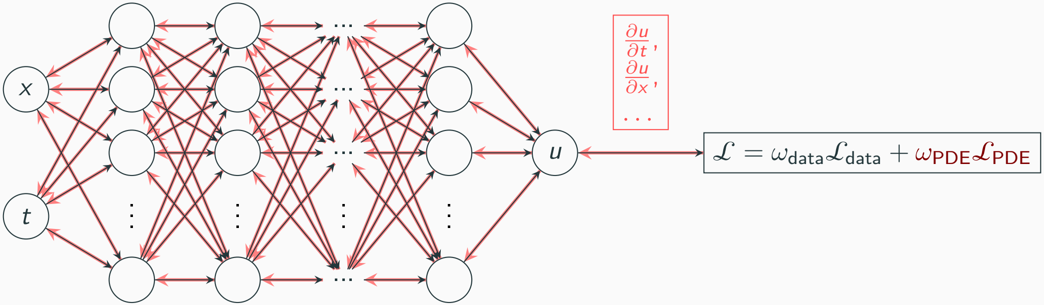

# Advantages and Drawbacks of PINNs

## Advantages

- **Mesh free**
- **Mostly unsupervised** and work with **incomplete models** (e.g., we learn only the missing physics) and **imperfect data**.
- Strong generalization properties with **small data** due to **embedded physics**.
- **High dimensional problems** (PDEs like Black-Scholes, Allen-Cahn).
- Solve **inverse and forward problems**, stationary and time-dependent, assimilate data in the **same way**.

## Drawbacks

- **Large computational cost** associated with the training of the neural networks.
- Generally, the training process is **not robust** and **depends heavily on well-chosen weights**
- **Convergence** properties **not well-understood**.
- **Poor scaling** to large domains.
- Learning high frequencies (**spectral bias**) / multi-scale solutions is **difficult**.

# Epidemic Parameter Identification Using Physics-Informed Neural Networks

## SEIR model

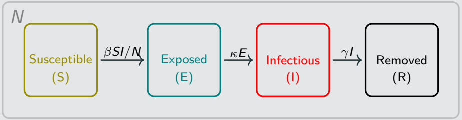


We consider the system of ODEs

$$
\begin{aligned}
\frac{dS}{dt} &= -\beta \frac{S\, I}{N} \\
\frac{dE}{dt} &= \beta \frac{S\, I}{N} - \kappa\, E \\
\frac{dI}{dt} &= \kappa\, E - \gamma\, I \\
\frac{dR}{dt} &= \gamma\, I
\end{aligned}
$$

with initial values $S(t_0) \geq 0, E(t_0) \geq 0, I(t_0) \geq 0$, and $R(t_0) \geq 0$ at some initial time $t_0$. The infective period $\gamma$ and the exposed period $1/\kappa$ are given.

$\rightarrow$ **Identify the time-dependent contact rate $\beta$** from given data for $S$, $E$, and $I$.

## Parameter identification using PINNs

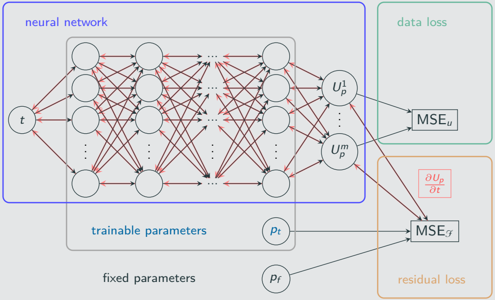


Training the weights $W$ and bias $b$ of the the neural work and the contact rate $\beta$ by **minimizing the mean-squared data error (MSDE) and the mean-squared residual error (MSRE)**:

$$\arg \min_{W,b,\beta} \left( \underbrace{\text{MSE}_U^{W,b}}_{\text{MSDE}} + \underbrace{\text{MSE}_{\mathcal{F}_p}^{W,b}}_{\text{MSRE}} \right)$$

## Results for synthetic data

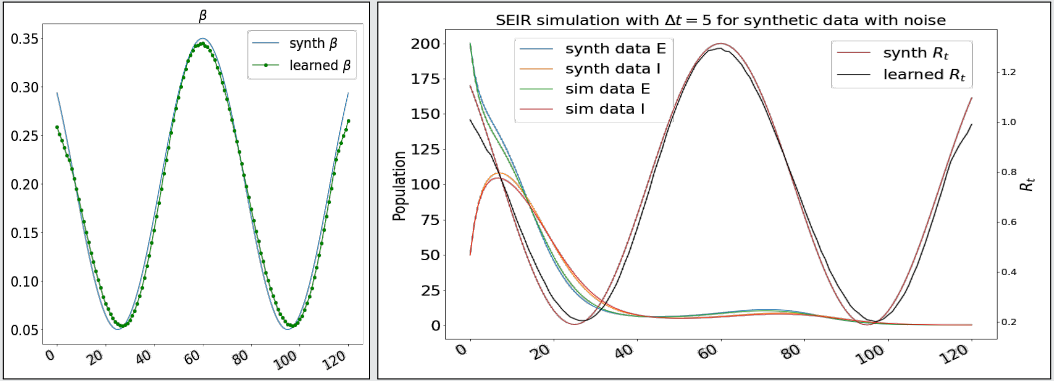


*synth data* and *sim data* are obtained by simulating the SEIR model with *synth* $\beta$ and *learned* $\beta$, respectively.

Cf. Grimm, Heinlein, Klawonn, Lanser, Weber (2022).

## Results for real data for COVID-19 (Germany)

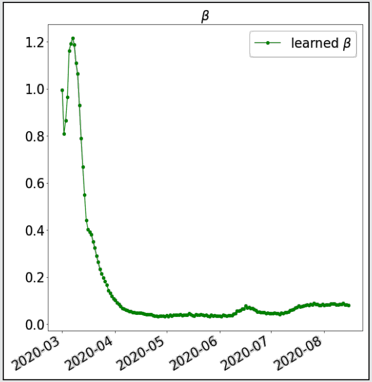


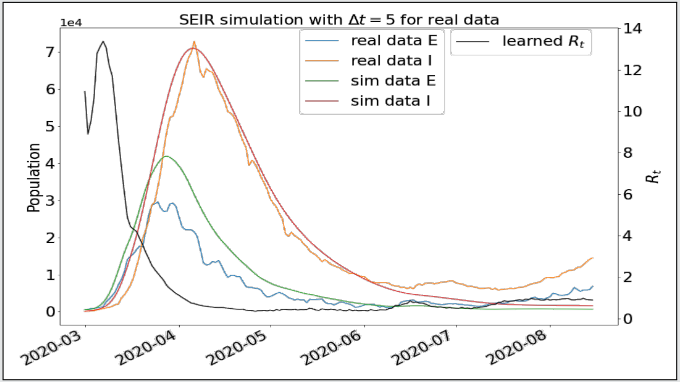


*real data* and *sim data* are obtained by simulating the SEIR model with *real* $\beta$ and *learned* $\beta$, respectively.

Cf. **Grimm, Heinlein, Klawonn, Lanser, Weber (2022)**.

# Domain decomposition-based training strategies for PINNs

# Scaling Issues in Neural Network Training

- **Spectral bias:** Neural networks prioritize learning lower frequency functions first irrespective of their amplitude.

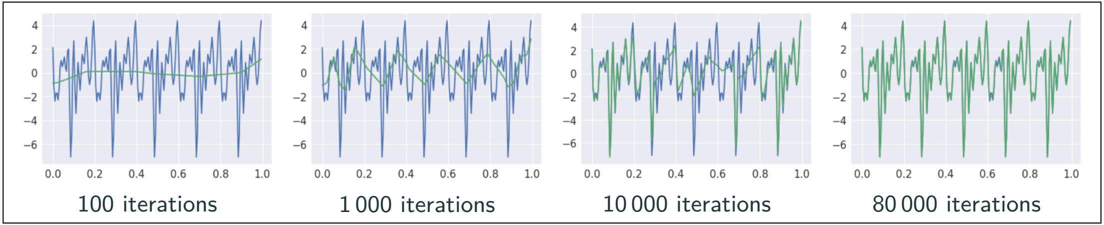


**Rahaman, N., et al,** *On the spectral bias of neural networks. 36th International Conference on Machine Learning*, **ICML (2019)**

- Solving solutions on large domains and/or with multiscale features potentially requires **very large neural networks**.
- Training may **not sufficiently reduce the loss** or take **large numbers of iterations**.
- Significant **increase on the computational work**

# Domain Decomposition Methods

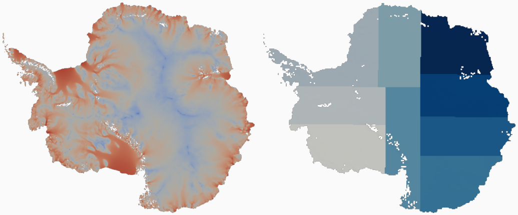

Images based on Heinlein, Perego, Rajamanickam (2022)

**Idea**

**Decomposing** a large **global problem** into smaller **local problems**:

- Better **robustness** and **scalability** of numerical solvers
- Improved **computational efficiency**
- Introduce **parallelism**

**Historical remarks:** The **alternating Schwarz method** is the earliest **domain decomposition method (DDM)**, which has been invented by **H. A. Schwarz** and published in **1870**:

- Schwarz used the algorithm to establish the **existence of harmonic functions** with prescribed boundary values on **regions with non-smooth boundaries**.

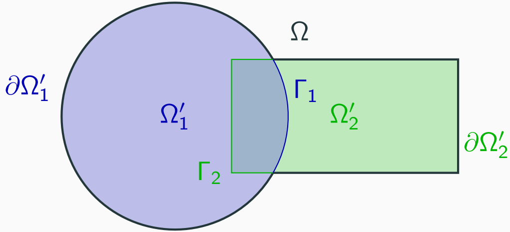

# Machine Learning and Domain Decomposition Methods

A **non-exhaustive overview**:

- **Machine Learning-enhanced adaptive FETI–DP** (finite element tearing and interconnecting – dual primal): Heinlein, Klawonn, Lanser, Weber (2019)
- **D3M** (deep domain decomposition method): Li, Tang, Wu, and Liao (2019)
- **DeepDDM** (deep-learning-based domain decomposition method): Li, Xiang, Xu (2020)
- **Two-Level DeepDDM**: Mercier, Gratton (arXiv 2021)
- **cPINNs** (conservative physics-informed neural networks): Jagtap, Kharazmi, and Karniadakis (2020)
- **XPINNs** (extended physics-informed neural networks): Jagtap, Karniadakis (2020)
- **FBPINNs** (finite basis physics-informed neural networks): Moseley, Markham, and Nissen-Meyer (arXiv 2021)

An overview of the state-of-the-art in early 2021:

A. Heinlein, A. Klawonn, M. Lanser, J. Weber.
**Combining machine learning and domain decomposition methods for the solution of partial differential equations — A review.**
GAMM-Mitteilungen. 2021.

The **FBPINN** (finite basis physics-informed neural networks) approach has been proposed in **Moseley, Markham, and Nissen-Meyer (arXiv 2021)**.

Solve

$$
\begin{aligned}
\frac{du}{dx} &= \cos(\omega x), \\
u(0) &= 0,
\end{aligned}
$$

for different values of $\omega$.

**Scaling issues**

- Size of the computational domain
- Size of frequencies

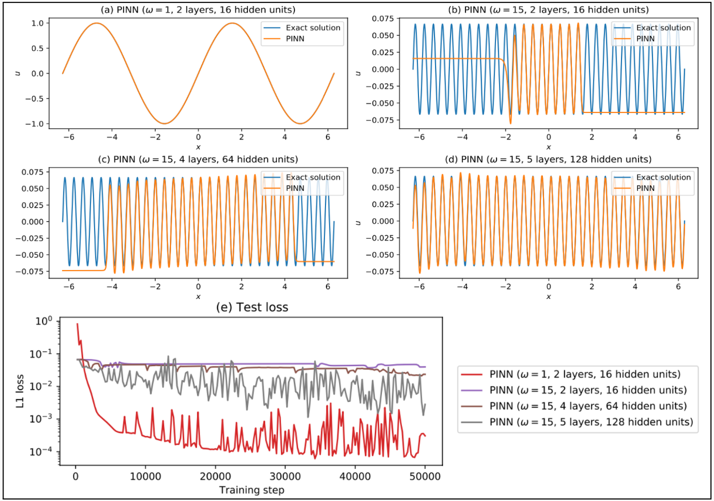


(a) 321 free parameters (d) 66 433 free parameters

# Finite Basis Physics-Informed Neural Networks (FBPINNs)

In the **finite basis physics informed neural network (FBPINNs) method** introduced in Moseley, Markham, and Nissen-Meyer (arXiv 2021), we solve the boundary value problem

$$
\begin{aligned}
\mathcal{N}[u](\boldsymbol{x}) &= f(\boldsymbol{x}), & \boldsymbol{x} \in \Omega \subset \mathbb{R}^d, \\
\mathcal{B}_k[u](\boldsymbol{x}) &= g_k(\boldsymbol{x}), & \boldsymbol{x} \in \Gamma_k \subset \partial\Omega.
\end{aligned}
$$

using neural networks, we employ the **PINN** approach and **enforce the boundary conditions using a constraining operator**, similar to Lagaris et al. (1998).

## Weak enforcement of boundary conditions

Loss function

$$\mathcal{L}(\boldsymbol{\theta}) = w_I \mathcal{L}_{\text{PDE}} + w_B \mathcal{L}_{\text{BC}},$$

where

$$
\begin{aligned}
\mathcal{L}_{\text{PDE}}(\boldsymbol{\theta}) &= \frac{1}{N_I} \sum_{i=1}^{N_I} \left(\mathcal{N}[u](\mathbf{x}_i, \boldsymbol{\theta}) - f(\mathbf{x}_i)\right)^2, \\
\mathcal{L}_{\text{BC}}(\boldsymbol{\theta}) &= \frac{1}{N_{\text{B}}} \sum_{i=1}^{N_{\text{B}}} \left(\mathcal{B}_k[u](\mathbf{x}_i, \boldsymbol{\theta}) - g_k(\mathbf{x}_i)\right)^2.
\end{aligned}
$$

## Hard enforcement of boundary conditions

Loss function

$$\mathcal{L}(\boldsymbol{\theta}) = \frac{1}{2} \sum_{i=1}^{N_I} \left(\mathcal{N}[\mathcal{C}u](\mathbf{x}_i, \boldsymbol{\theta}) - f(\mathbf{x}_i)\right)^2,$$

with constraining operator $\mathcal{C}$, which explicitly enforces the boundary conditions.

$\rightarrow$ Often **improves training performance**

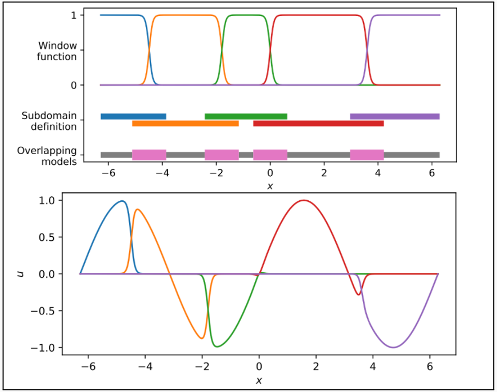


- Domain decomposition: $\Omega = \cup_{j=1}^{J} \Omega_j$
- Collocation points (global): $\{x_i\}_{i=1}^{N}$
- Overlapping/interior parts $\Omega_j^{\circ}$ and $\Omega_j^{int}$
- Local solutions $u_j$, window functions $w_j$
- Global solution $\mathcal{C}u = \mathcal{C} \sum_{j, x_i \in \Omega_j} \omega_j u_j$

Global loss function

$$\mathcal{L}(\boldsymbol{\theta}_1, \ldots, \boldsymbol{\theta}_J) = \underbrace{\frac{1}{N} \sum_{j=1}^{J} \sum_{\mathbf{x}_i \in X_j^{\circ}} \left( \mathcal{N}[\mathcal{C} \sum_{l, \mathbf{x}_i \in X_l} \omega_l u_l](\mathbf{x}_i, \boldsymbol{\theta}_l) - f(\mathbf{x}_i) \right)^2}_{=:\mathcal{L}^{\circ}(\boldsymbol{\theta}_1, \ldots, \boldsymbol{\theta}_J)}$$

$$+ \underbrace{\frac{1}{N} \sum_{j=1}^{J} \sum_{\mathbf{x}_i \in X_j^{int}} \left( \mathcal{N}[\mathcal{C} \sum_{l, \mathbf{x}_i \in X_l} \omega_l u_l](\mathbf{x}_i, \boldsymbol{\theta}_l) - f(\mathbf{x}_i) \right)^2}_{=:\mathcal{L}^{int}(\boldsymbol{\theta}_1, \ldots, \boldsymbol{\theta}_J)}.$$

Since $X_i^{int} \cap X_j^{int} = \emptyset$ for $i \neq j$,

$$\mathcal{L}^{int}(\boldsymbol{\theta}_1, \ldots, \boldsymbol{\theta}_J) = \frac{1}{N} \sum_{j=1}^{J} \sum_{\mathbf{x}_i \in X_j^{int}} \left( \mathcal{N}[\mathcal{C} \omega_j u_j](\mathbf{x}_i, \boldsymbol{\theta}_j) - f(\mathbf{x}_i) \right)^2$$

- The subdomains can be split active (trained in parallel) and inactive (fixed)
- This corresponds to classical parallel (all active) or multiplicative (one active at a time)

# FBPINN With Flexible Scheduling

**Algorithm 1:** FBPINN training step

**if** $j \in \mathcal{A}$ *($\Omega_j$ is an active domain)* **then**

Perform $p$ iterations of gradient descent on $\boldsymbol{\theta}_j$ ($\boldsymbol{\theta}_l^k, l \neq j$ are kept fixed): $\boldsymbol{\theta}_j^{k+l} = \boldsymbol{\theta}_j^{k+l-1} - \lambda \nabla_{\boldsymbol{\theta}_j} \mathcal{L}(\boldsymbol{\theta}_1^k, \ldots, \boldsymbol{\theta}_j^{k+l-1}, \ldots, \boldsymbol{\theta}_J^k), l = 1, .., p.$

Update the solutions in the overlap (communication with the neighbors): $\forall \mathbf{x} \in \Omega_j^\circ,\ u(\mathbf{x}, \boldsymbol{\theta}_j^{k+p}) \leftarrow \sum_{l, \mathbf{x} \in \Omega_l} \omega_l u_l(\mathbf{x}, \boldsymbol{\theta}_l^{k+p}).$

Apply the constraining operator $u(\mathbf{x}, \boldsymbol{\theta}_j^k) \leftarrow \mathcal{C}(u(\mathbf{x}, \boldsymbol{\theta}_j^{k+p})).$

**end**

**Summary**

- Communication every $p$ iterations (better for overall efficiency)
- Multiplication with a window function : a way to restrict to the local domain.
- The set of active domains can be changed after the local training is completed.

# FBPINNs – Weak Scaling Study

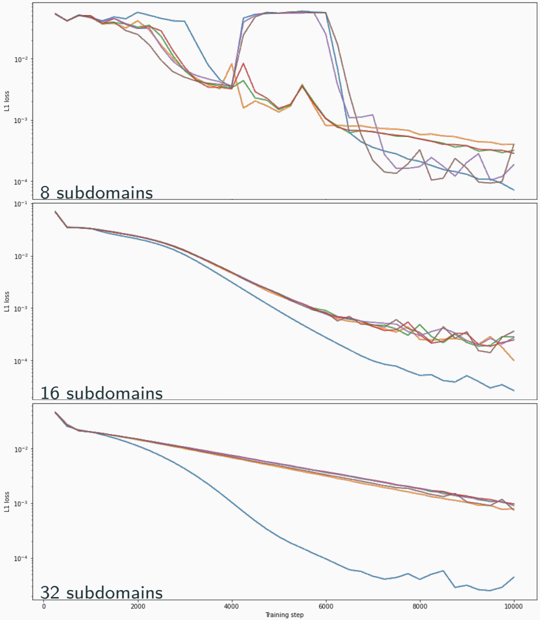


Solve, for $\omega = 15$,

$$\frac{du}{dx} = \cos(\omega x), \quad u(0) = 0.$$

- Fixed local network size and number of local collocation points. Then, we **increase the number of subdomains**.
- We choose all subdomains as active and test the influence of


## Observations

- Convergence get worse with an increasing number of subdomains
- No noticeable difference depending on how often we update, unless we update every iteration

# Two-Level FBPINN Algorithm

## Coarse correction and spectral bias

**Questions:**

- Scalability requires **global transport of information**. In domain decomposition, this is typically done using a **coarse global problem**.
- What does this mean in the **context of network training**?

**Idea:**

→ Learn low frequencies using a **small global network**, train high frequencies using local networks.

Investigate this for a **simple model problem** with **two frequencies**

$$\begin{cases} \frac{du}{dx} &= \omega_1 \cos(\omega_1 x) + \omega_2 \cos(\omega_2 x) \\ u(0) &= 0. \end{cases}$$

with $\omega_1 = 1$, $\omega_2 = 15$,

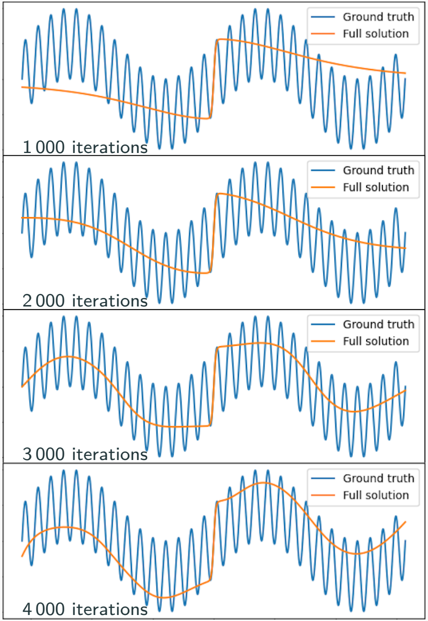

Now, **learn the error (higher frequencies)** using the **one-level FBPINN model** using **local models on 30 subdomains**.

Overlapping domain decomposition into 30 subdomains

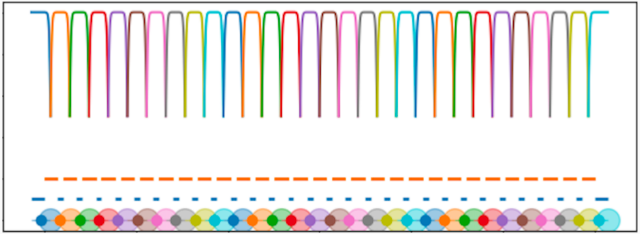

Local and coarse models

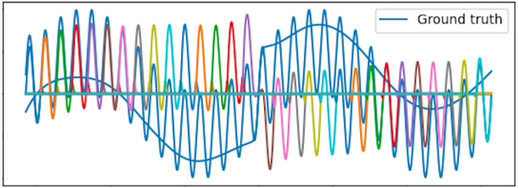


Two-level model

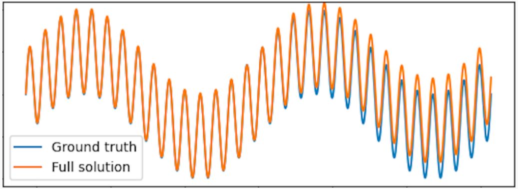

# Surrogate models for computational fluid dynamics simulations
# Data-driven approach

# Computational Fluid Dynamics (CFD) Simulations Are Time Consuming

In **Giese, Heinlein, Klawonn, Knepper, Sonnabend (2019)**, a benchmark for **comparing MRI measurements and CFD simulations** of hemodynamics in **intracranial aneurysms** was proposed.

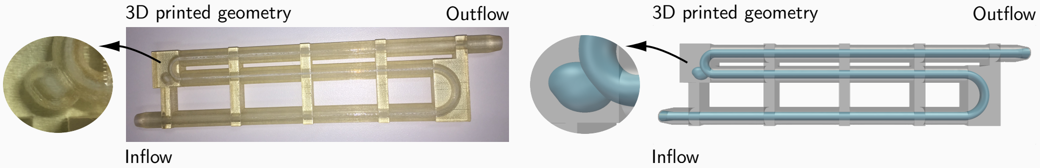


To obtain accurate simulation results, simulations with $\approx 10\,\mathrm{m}$ d.o.f.s were carried out. On $O(100)$ MPI ranks, the computation of a steady state took $O(1)\,\mathrm{h}$ on CHEOPS supercomputer at UoC.

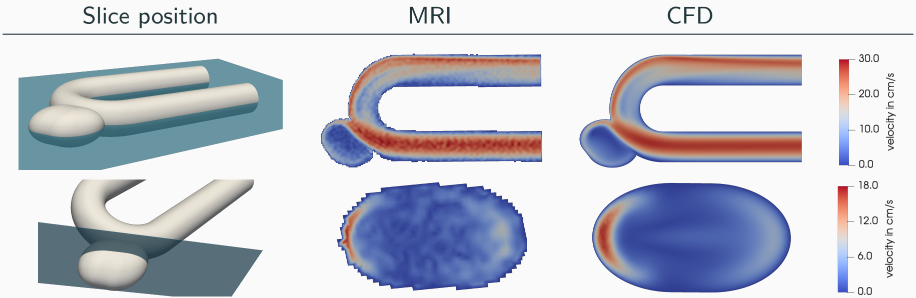

# Computational Fluid Dynamics (CFD) Simulations Are Time Consuming

In **Giese, Heinlein, Klawonn, Knepper, Sonnabend (2019)**, a benchmark for **comparing MRI measurements and CFD simulations** of hemodynamics in **intracranial aneurysms** was proposed.

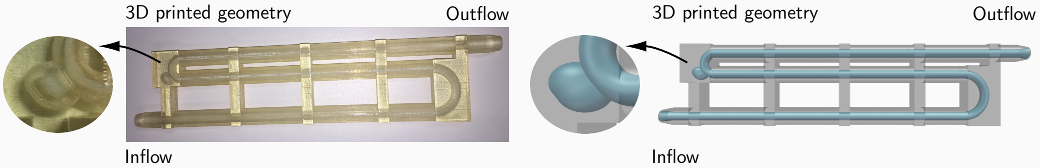


To obtain accurate simulation results, simulations with $\approx 10\,\mathrm{m}$ d.o.f.s were carried out. On $O(100)$ MPI ranks, the computation of a steady state took $O(1)\,\mathrm{h}$ on CHEOPS supercomputer at UoC.

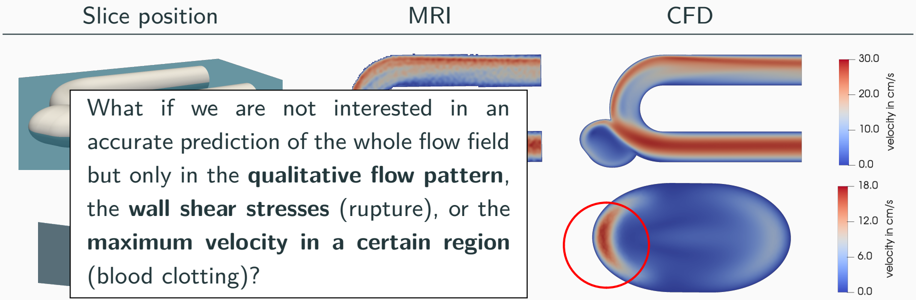


What if we are not interested in an accurate prediction of the whole flow field but only in the **qualitative flow pattern**, the **wall shear stresses** (rupture), or the **maximum velocity in a certain region** (blood clotting)?

# Using PINNs as Surrogate Models

Learning the solution of one specific boundary value problem (BVP), for instance, using PINNs

$$
\begin{aligned}
\mathcal{N}[u](\boldsymbol{x}) &= f(\boldsymbol{x}), && \boldsymbol{x} \in \Omega \subset \mathbb{R}^d, \\
\mathcal{B}_k[u](\boldsymbol{x}) &= g_k(\boldsymbol{x}), && \boldsymbol{x} \in \Gamma_k \subset \partial\Omega,
\end{aligned}
$$

generally **requires re-training the model once the boundary problem changes**.

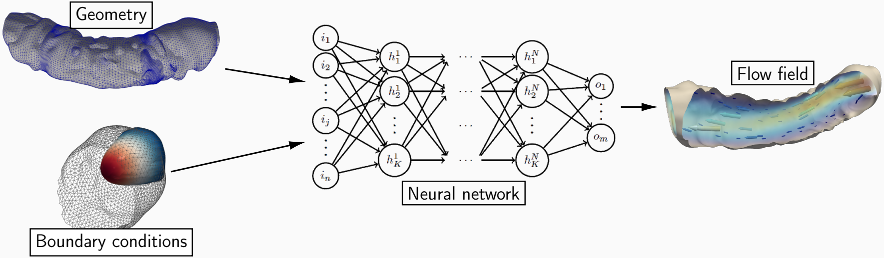


Instead, we are interested in a **single surrogate model** that can predict the solution for a variety of

- **geometries**,
- **initial and boundary conditions**, and/or
- **material parameters**.

# Operator Learning and Surrogate Modeling

Our approach is inspired by the work **Guo, Li, Iorio (2016)**, in which **convolutional neural networks (CNNs)** are employed to predict the flow in channel with an obstacle.

In particular, we use a pixel image of the **geometry as input** and predict an image of the resulting **stationary flow field as output**:

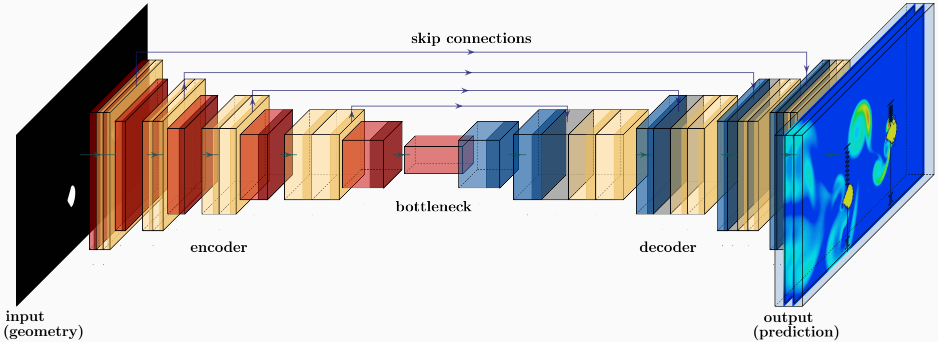

# Operator Learning and Surrogate Modeling

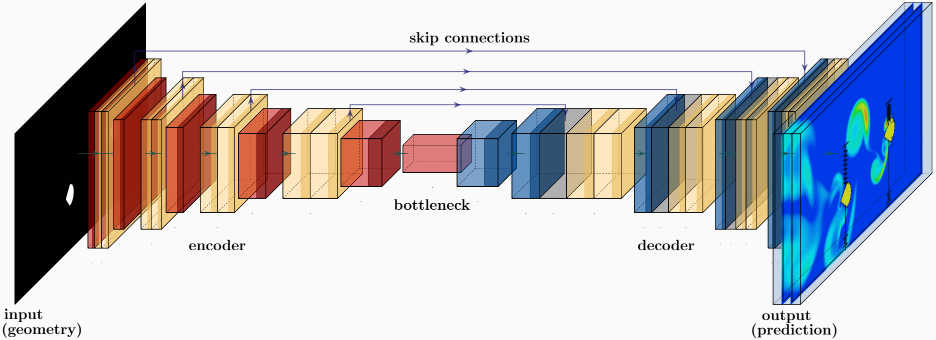


We learn the **nonlinear map** between a **representation space of the geometry** and the **solution space** of the stationary Navier–Stokes equations → **Operator Learning**.

### Operator learning

Learning **maps between function spaces**, e.g.,

- between the right-hand side and the solution of a BVP.

### Other operator learning approaches

- **DeepOnet:** Lu, Jin, and Karniadakis. (arXiv preprint 2019).
- **Neural operators:** Kovachki, Li, Liu, Azizzadenesheli, Bhattacharya, Stuart, and Anandkumar (arXiv preprint 2021).

# Model Problem – Flow Around an Obstacle in Two Dimensions

We propose a **simple model problem** to investigate predictions of a **steady flow in a channel with an obstacle**; our approach is inspired by **Guo, Li, Iorio (2016)**.

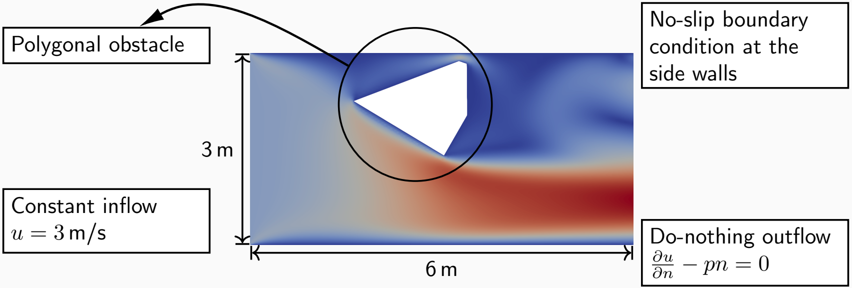


In particular, we restrict ourselves to

→ a **simple rectangular basic geometry** and

→ **fixed boundary conditions**.

However, we **vary the geometry of the polygonal obstacle**. In addition, we **interpolate the input and output data to a structured tensor product mesh** to impose a structure.

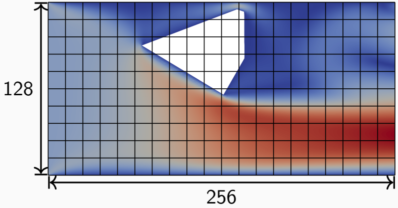

# Type I – III Geometries (Eichinger, Heinlein, Klawonn (2021, 2022))

We first consider **obstacles** of the following three types; see also Guo, Li, Iorio (2016) for a similar approach. In particular, we **randomly generate star-shaped polygons with 3, 4, 5, 6, and 12 edges**.

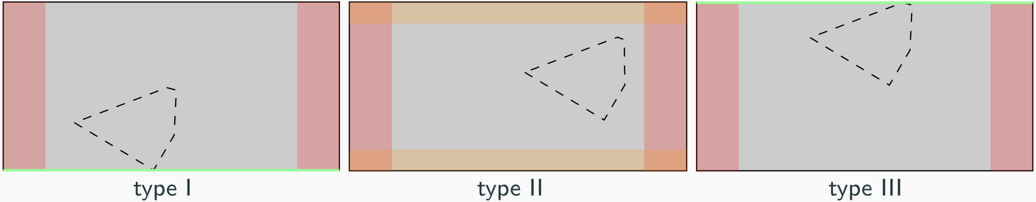


First, we consider **100 000 pairs of geometry and flow data** (90 000 training; 10 000 validation) for **Type I (50 000) & Type II (50 000)**. Later, we will also consider Type III.

# Computation of the Flow Data Using OpenFOAM®

We solve the **steady Navier-Stokes equations**

$$
\begin{aligned}
-\nu\Delta\vec{u} + (u\cdot\nabla)\,\vec{u} + \nabla p &= 0 \text{ in } \Omega \\
\nabla\cdot u &= 0 \text{ in } \Omega,
\end{aligned}
$$

where $\vec{u}$ and $p$ are the velocity and pressure fields and $\nu$ is the viscosity. Furthermore, we prescribe the previously described boundary conditions.

## Software pipeline

1. Define the boundary of the polygonal obstacle and **create the corresponding STL (standard triangulation language) file**.
2. **Generate a hexahedral compute grid** (`snappyHexMesh`).
3. Run the **CFD simulation** (`simpleFoam`).
4. **Interpolate geometry information and flow field** onto a pixel grid.
5. **Train the CNN**.

## Input data

**Binary**

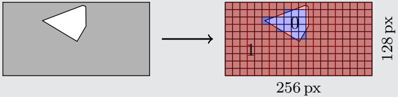


**SDF (Signed Distance Function)**

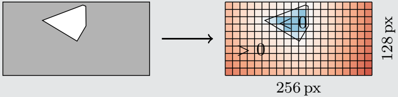


## Output data

$u_x$

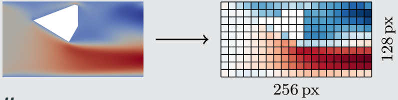


$u_y$

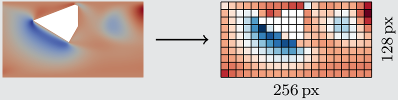

**Bottleneck CNN** (Guo, Li, Iorio (2016))

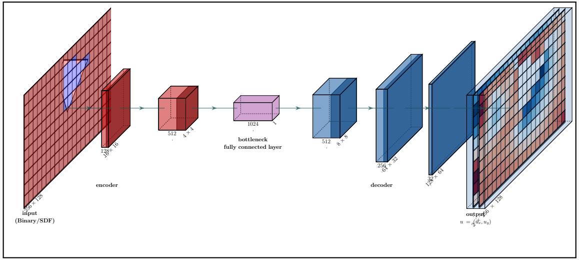


**U-Net** (Ronneberger, Fischer, Brox (2015))

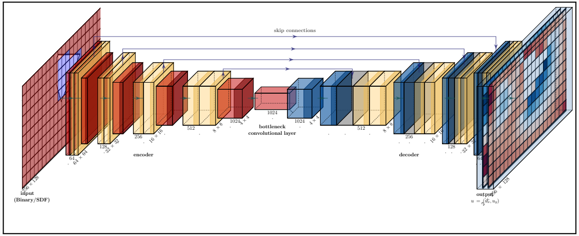


**One decoder**

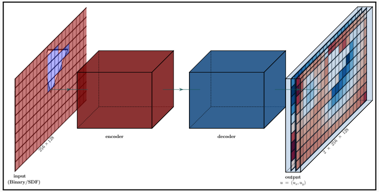


**Two decoders**

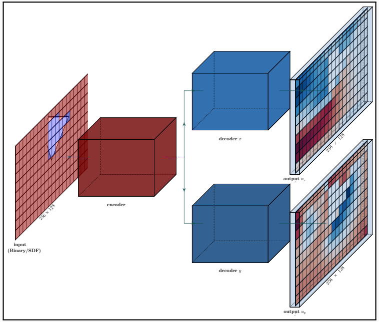

# Comparison CFD Vs NN (Relative Error 2 %)

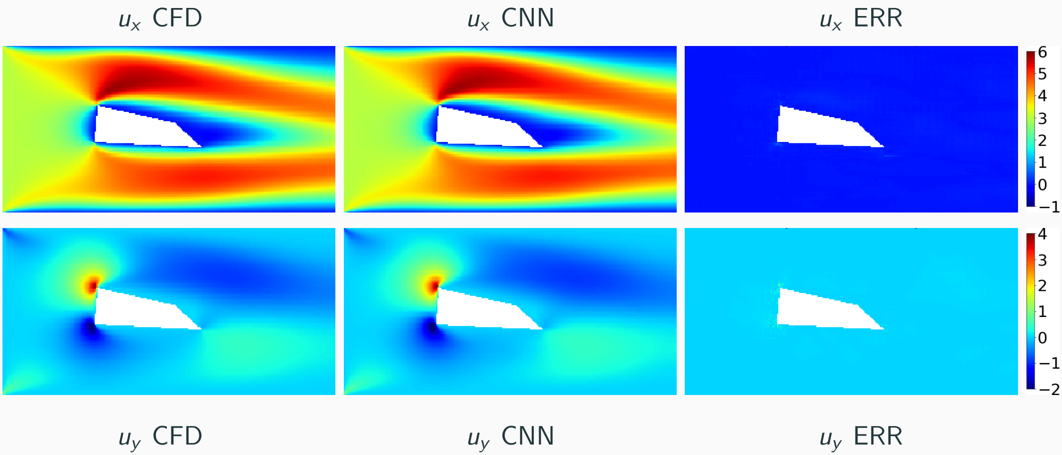


Cf. **Eichinger, Heinlein, Klawonn (2021, 2022)**

# Comparison CFD Vs NN (Relative Error 14 %)

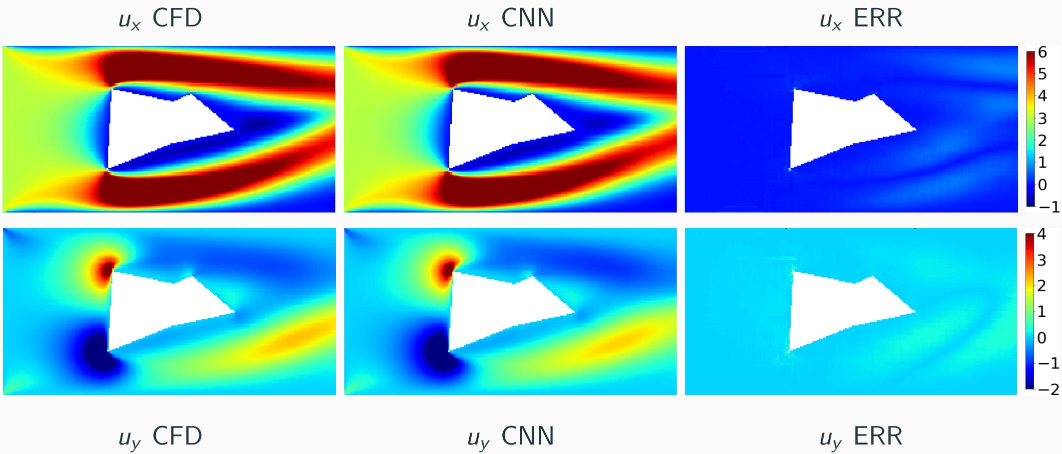


Cf. **Eichinger, Heinlein, Klawonn (2021, 2022)**

# Comparison CFD Vs NN (Relative Error 31 %)

$u_x$ CFD $\quad$ $u_x$ CNN $\quad$ $u_x$ ERR

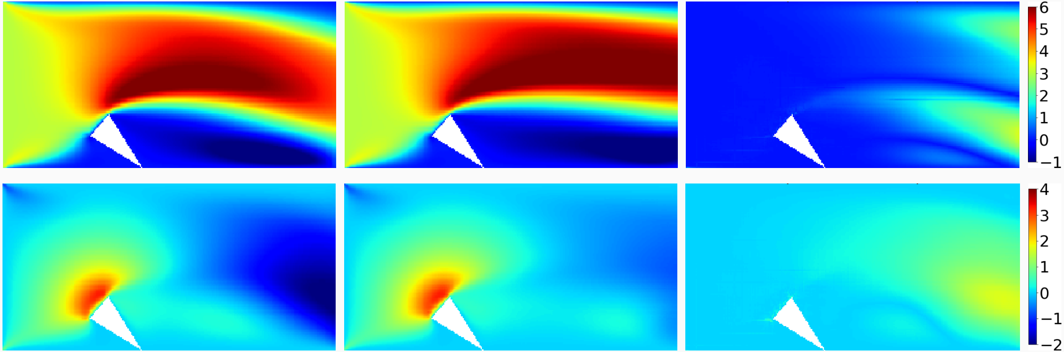


$u_y$ CFD $\quad$ $u_y$ CNN $\quad$ $u_y$ ERR

Cf. **Eichinger, Heinlein, Klawonn (2021, 2022)**

# First Results (Eichinger, Heinlein, Klawonn (2021, 2022))

We compare the **relative error (RE)** $\frac{\|u_{i,j}-\hat{u}_{i,j}\|_2}{\|u_{i,j}\|_2+10^{-4}}$ **averaged over all non-obstacle pixels** and **all validation data configurations**. Furthermore: **MSE = mean squared error**; **MAE = mean absolute error**.

| | | | Bottleneck CNN (Guo, Li, Iorio (2016)) | | | U-Net (Ronneberger, Fischer, Brox (2015)) | | |
|---|---|---|---|---|---|---|---|---|
| input | # dec. | loss | total | type I | type II | total | type I | type II |
| SDF | 1 | MSE | **61.16 %** | 110.46 % | 11.86 % | 17.04 % | 29.42 % | 4.66 % |
| | | MSE + RE | 3.97 % | 3.31 % | **4.63 %** | 2.67 % | 2.11 % | 3.23 % |
| | | MAE | 25.19 % | 41.52 % | 8.86 % | 9.10 % | 13.89 % | 4.32 % |
| | | MAE + RE | 4.45 % | 3.84 % | 5.05 % | 2.48 % | 1.87 % | **3.10 %** |
| | 2 | MSE | 49.82 % | 89.12 % | 10.51 % | 13.01 % | 21.59 % | 4.42 % |
| | | MSE + RE | **3.85 %** | **3.05 %** | 4.64 % | **2.43 %** | **1.78 %** | 3.23 % |
| | | MAE | 45.23 % | 81.38 % | 9.08 % | 5.47 % | 7.06 % | 3.89 % |
| | | MAE + RE | 4.33 % | 3.74 % | 4.91 % | 2.57 % | 1.98 % | 3.17 % |
| Binary | 1 | MSE | 49.78 % | 88.28 % | 11.28 % | 27.15 % | 49.15 % | 5.15 % |
| | | MSE + RE | 10.12 % | 11.44 % | 8.80 % | 5.49 % | 6.25 % | 4.74 % |
| | | MAE | 39.16 % | 64.77 % | 13.54 % | 15.69 % | 26.36 % | 5.02 % |
| | | MAE + RE | 10.61 % | 12.34 % | 8.87 % | **4.48 %** | **5.05 %** | **3.90 %** |
| | 2 | MSE | **51.34 %** | 91.20 % | 11.48 % | 24.00 % | 43.14 % | 4.85 % |
| | | MSE + RE | 10.03 % | 11.37 % | 8.69 % | 5.56 % | 6.79 % | 4.33 % |
| | | MAE | 37.16 % | 62.01 % | 12.32 % | 21.54 % | 38.12 % | 4.96 % |
| | | MAE + RE | **9.53 %** | **10.91 %** | **8.15 %** | 6.04 % | 7.88 % | 4.20 % |

We test the **generalization properties** of our **previously trained U-Net**. In particular, we predict the flow for new geometries of **Type I** and **Type II**; 1 000 geometries each (500 Type I & 500 Type II).

| # polygon edges | SDF input | | | Binary input | | |
|---|---|---|---|---|---|---|
| | total | type I | type II | total | type I | type II |
| 7 | 2.71 % | 1.89 % | 3.53 % | 4.39 % | 4.61 % | 4.16 % |
| 8 | 2.82 % | 1.98 % | 3.65 % | 4.67 % | 4.89 % | 4.44 % |
| 10 | 3.21 % | 2.32 % | 4.10 % | 5.23 % | 5.51 % | 4.94 % |
| 15 | 4.01 % | 3.16 % | 4.86 % | 7.76 % | 7.85 % | 6.66 % |
| 20 | 5.08 % | 4.22 % | 5.93 % | 9.70 % | 10.43 % | 8.97 % |

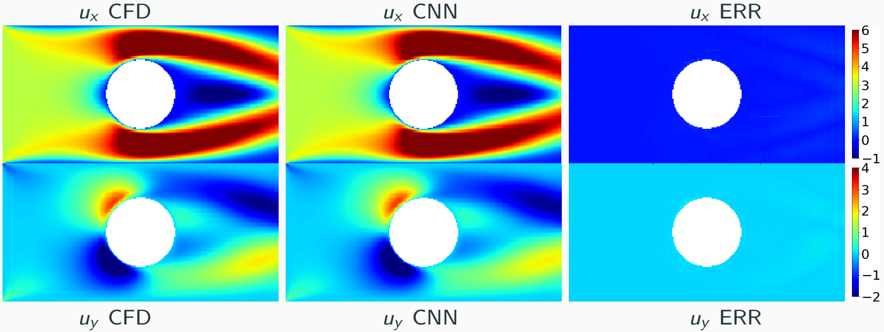

# Generalization Issues – Type III Geometry (Relative Error 158 %)

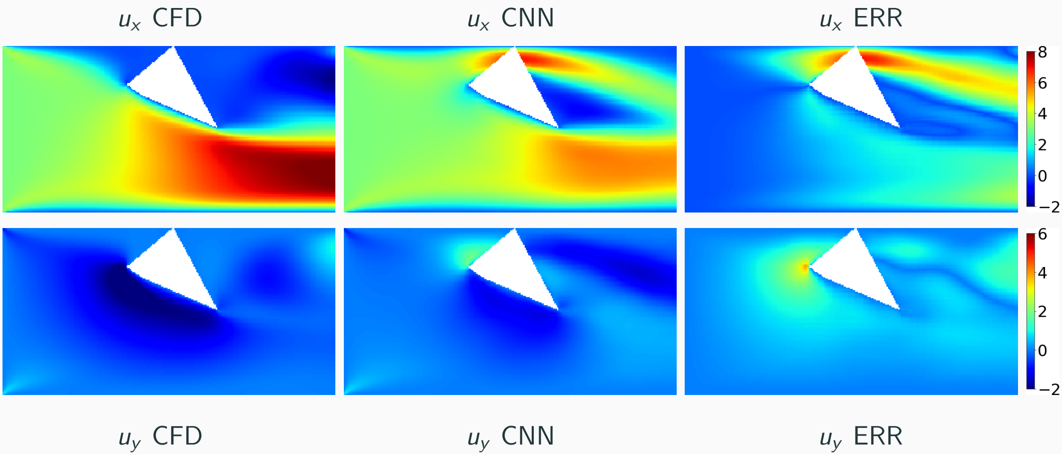


Cf. **Eichinger, Heinlein, Klawonn (2022)**

# Transfer Learning – Type III Geometries

The **best model (U-Net, one decoder, MAE+RE loss)** trained on type I and type II geometries **performs poorly on 2 500 type III geometries**:

| | SDF Input | binary Input |
|---|---|---|
| **type III** | **22 985.89 %** | **4 134.69 %** |

We compare the following approaches to generalize to type III geometries:

- **Approach 1:** Train a new model from scratch on type III geometries (2 500 training + 2 500 validation data)
- **Approach 2:** Train the previous model on type III geometries
- **Approach 3:** Train the previous model on a data set consisting of the old data (type I & type II) and type III data

| | | type I & II | | type III | |
|---|---|---|---|---|---|
| learning approach | # training epochs | SDF input | binary input | SDF input | binary input |
| 1 | 100 | - | - | 98.02 % | 111.75 % |
| 2 | 100 | 208.02 % | 105.43 % | 7.18 % | 11.81 % |
| 3 | 3 | **3.33 %** | **7.06 %** | **4.94 %** | **11.28 %** |

Neural networks **forget if data is removed from the training data**. However, **new geometries (type III: symmetric to Type I) can be learned quickly** if they are **added to the existing training data**.

# Computing Times

**Data:**

| | Avg. Runtime per Case (Serial) |
|---|---|
| Create STL | 0.15 s |
| `snappyHexMesh` | 37 s |
| `simpleFoam` | 13 s |
| **Total Time** | $\approx$ 50 s |

**Training:**

| | Bottleneck CNN | | U-Net | |
|---|---|---|---|---|
| # decoders | 1 | 2 | 1 | 2 |
| # parameters | $\approx$ 47 m | $\approx$ 85 m | $\approx$ 34 m | $\approx$ 53.5 m |
| time/epoch | **180 s** | **245 s** | **195 s** | **270 s** |

**Comparison CFD Vs NN:**

| | CFD (CPU) | NN (CPU) | NN (GPU) |
|---|---|---|---|
| **Avg. Time** | **50 s** | **0.092 s** | **0.0054 s** |

$\Rightarrow$ Flow predictions using neural networks may be less accurate and the **training phase expensive**, but the **flow prediction is** $\approx 5 \cdot 10^2 - 10^4$ **times faster**.

**CPU:** AMD Threadripper 2950X (8 $\times$ 3.8 Ghz), 32GB RAM; **GPU:** GeForce RTX 2080Ti

# Surrogate models for computational fluid dynamics simulations
# Physics-aware approach

# U-Net (Ronneberger, Fischer, Brox (2015)) Revisited

→ We further **improved the U-Net architecture** for our application.

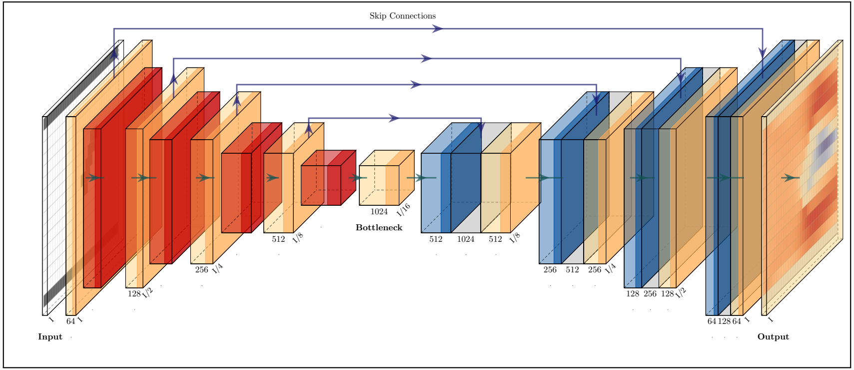


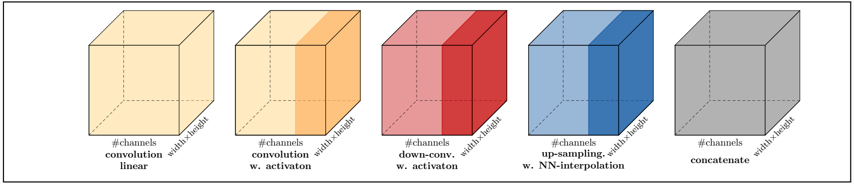

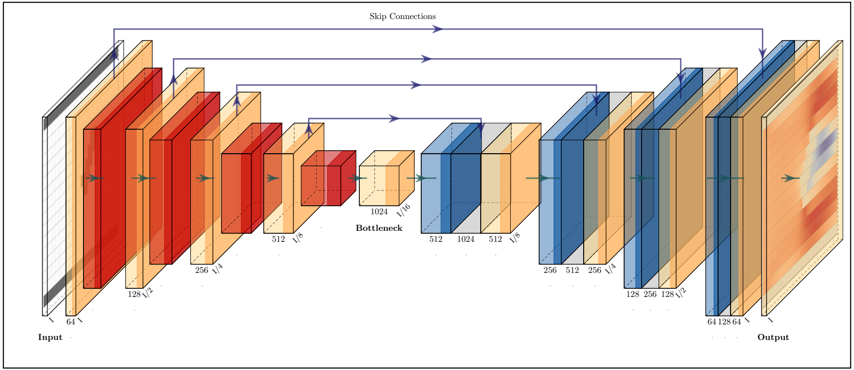


## Convolution

The action of a **convolutional layer** corresponds to **going over the image with a filter** (matrix):

$$\begin{pmatrix} a_{11} & a_{12} & a_{13} \\ a_{21} & a_{22} & a_{23} \\ a_{31} & a_{32} & a_{33} \end{pmatrix}$$

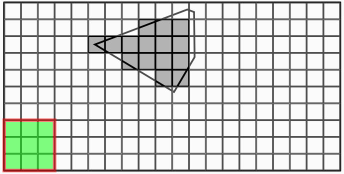

# U-Net (Ronneberger, Fischer, Brox (2015)) Revisited

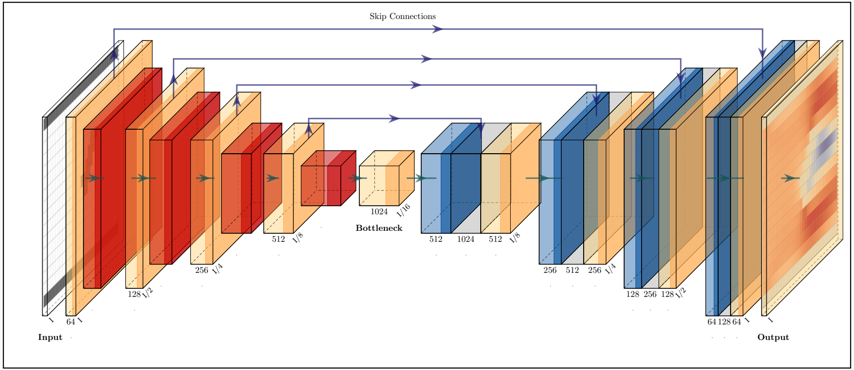


## Convolution

The action of a **convolutional layer** corresponds to **going over the image with a filter** (matrix):

$$\begin{pmatrix} a_{11} & a_{12} & a_{13} \\ a_{21} & a_{22} & a_{23} \\ a_{31} & a_{32} & a_{33} \end{pmatrix}$$

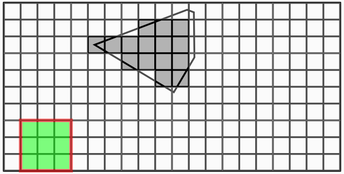

# U-Net (Ronneberger, Fischer, Brox (2015)) Revisited

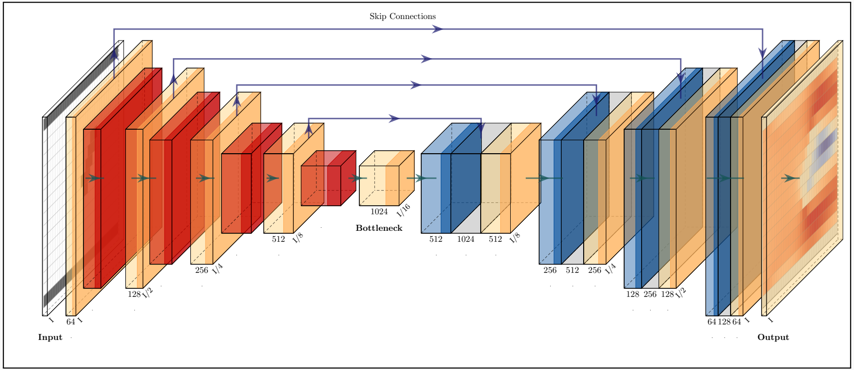


## Convolution

The action of a **convolutional layer** corresponds to **going over the image with a filter** (matrix):

$$\begin{pmatrix} a_{11} & a_{12} & a_{13} \\ a_{21} & a_{22} & a_{23} \\ a_{31} & a_{32} & a_{33} \end{pmatrix}$$

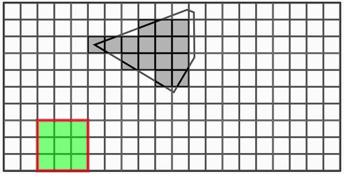

# Unsupervised Learning Approach – PDE Loss Using Finite Differences

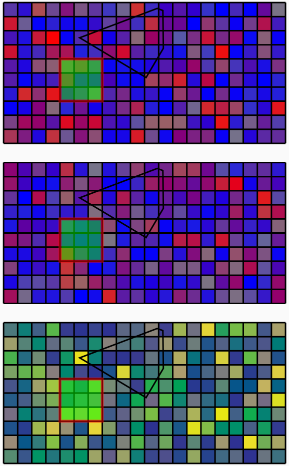

**Minimization of the mean squared residual** of the Navier-Stokes equations

$$\min_{u_{NN}, p_{NN}} \frac{1}{\#\text{pixels}} \sum_{\text{pixels}} \left\| \begin{matrix} F_{\text{mom}}(u_{NN}, p_{NN}) \\ F_{\text{mass}}(u_{NN}, p_{NN}) \end{matrix} \right\|^2$$

where $u_{NN}$ and $p_{NN}$ are the output images of our CNN and

$$\begin{aligned} F_{\text{mom}}(u,p) &:= -\nu \Delta \vec{u} + (u \cdot \nabla)\vec{u} + \nabla p, \\ F_{\text{mass}}(u,p) &:= \nabla \cdot u. \end{aligned}$$

We use a **finite difference discretization on the output pixel image** by defining filters on the last layer of the CNN-based on the stencils:

$$\frac{\partial}{\partial x} \quad \begin{matrix} 0 & 0 & 0 \\ -1 & 0 & 1 \\ 0 & 0 & 0 \end{matrix} \qquad \begin{matrix} 0 & 1 & 0 \\ 0 & 0 & 0 \\ 0 & -1 & 0 \end{matrix} \quad \frac{\partial}{\partial y}$$

$$\frac{\partial^2}{\partial x^2} \quad \begin{matrix} 0 & 0 & 0 \\ 1 & -2 & 1 \\ 0 & 0 & 0 \end{matrix} \qquad \begin{matrix} 0 & 1 & 0 \\ 0 & -2 & 0 \\ 0 & 1 & 0 \end{matrix} \quad \frac{\partial^2}{\partial y^2}$$

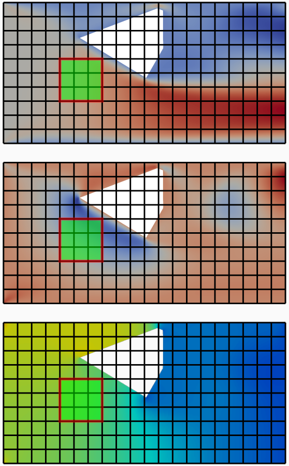

$$\left\| \begin{matrix} F_{\text{mom}}(u_{NN}, p_{NN}) \\ F_{\text{mass}}(u_{NN}, p_{NN}) \end{matrix} \right\|^2 >> 0$$

$$\left\| \begin{matrix} F_{\text{mom}}(u_{NN}, p_{NN}) \\ F_{\text{mass}}(u_{NN}, p_{NN}) \end{matrix} \right\|^2 \approx 0$$

Cf. **Grimm, Heinlein, Klawonn**

# Physics-Aware Approach – Boundary Conditions

The PDE loss can be minimized **without using simulation results as training data**.
Therefore, we also call this **physics-aware** approach **unsupervised**.

→ On a single geometry, this training of the neural network just corresponds to an **unconventional way of discretizing the Navier-Stokes equations using finite differences**.

Hence, we also have to **enforce the boundary conditions of our boundary value problem**:

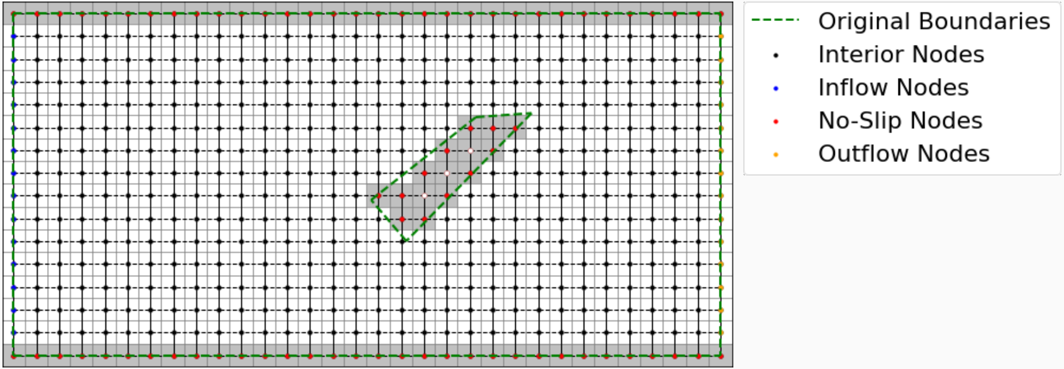

# Physics-Aware Approach – Single Geometry

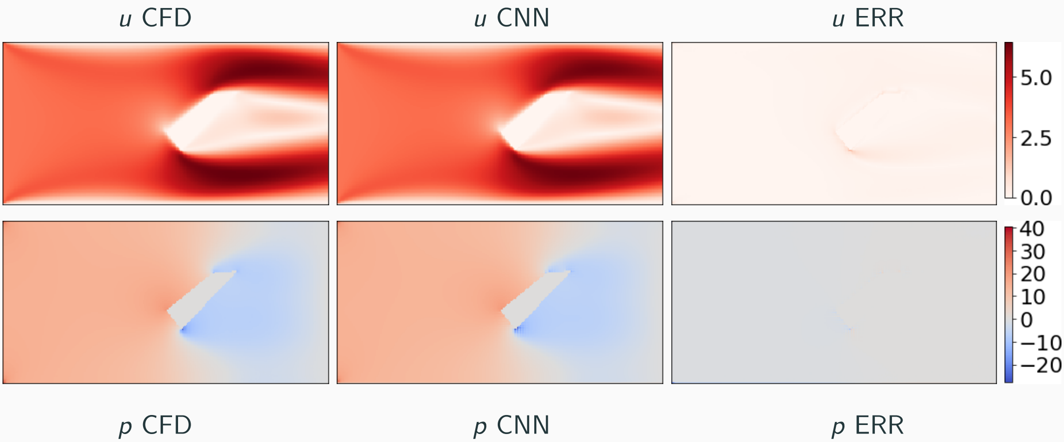

# Physics-Aware Approach – Single Geometry

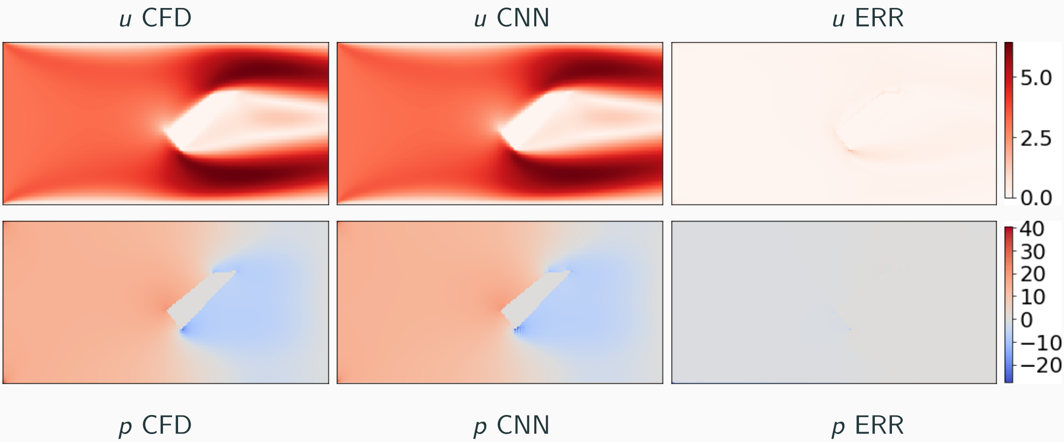


⇒ We can **solve the boundary value problem using a neural network**.

# Physics-Aware Approach – Single Geometry

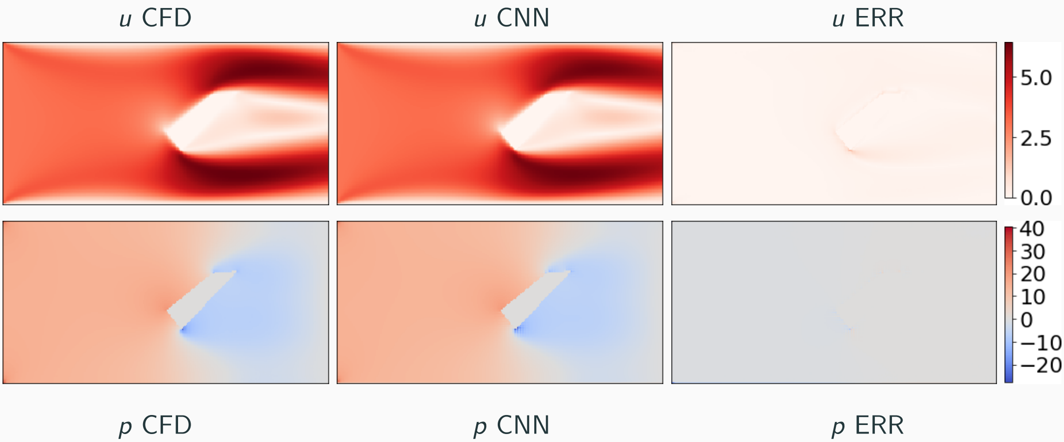


⇒ We can **solve the boundary value problem using a neural network**.

→ Now, we again build a **surrogate model for multiple geometries**.

# Results on $\approx$ 5 000 Type II Geometries

| | training data | error | $\frac{\|u_{NN}-u\|_2}{\|u\|_2}$ | $\frac{\|p_{NN}-p\|_2}{\|p\|_2}$ | mean residual momentum | mean residual mass | # epochs trained |
|---|---|---|---|---|---|---|---|
| **data-based** | 10% | train. | 2.07% | 10.98% | $1.1 \cdot 10^{-1}$ | $1.4 \cdot 10^{0}$ | 500 |
| | | val. | 4.48 % | 15.20 % | $1.6 \cdot 10^{-1}$ | $1.7 \cdot 10^{0}$ | |
| | 25% | train. | 1.93% | 8.45% | $9.1 \cdot 10^{-2}$ | $1.2 \cdot 10^{0}$ | 500 |
| | | val. | 3.49 % | 10.70 % | $1.2 \cdot 10^{-1}$ | $1.4 \cdot 10^{0}$ | |
| | 50% | train. | 1.48% | 8.75% | $9.0 \cdot 10^{-2}$ | $1.1 \cdot 10^{0}$ | 500 |
| | | val. | 2.70 % | 10.09 % | $1.1 \cdot 10^{-1}$ | $1.2 \cdot 10^{0}$ | |
| | 75% | train. | 1.43% | 7.30% | $1.0 \cdot 10^{-1}$ | $1.5 \cdot 10^{0}$ | 500 |
| | | val. | **2.52 %** | **8.67 %** | $1.2 \cdot 10^{-1}$ | $1.5 \cdot 10^{0}$ | |
| **physics-aware** | 10% | train. | 5.35% | 12.95% | $3.5 \cdot 10^{-2}$ | $7.8 \cdot 10^{-2}$ | 5 000 |
| | | val. | 6.72% | 15.39% | $6.7 \cdot 10^{-2}$ | $2.0 \cdot 10^{-1}$ | |
| | 25% | train. | 5.03% | 12.26% | $3.2 \cdot 10^{-2}$ | $7.3 \cdot 10^{-2}$ | 5 000 |
| | | val. | 5.78 % | 13.38 % | $5.3 \cdot 10^{-2}$ | $1.4 \cdot 10^{-1}$ | |
| | 50% | train. | 5.81% | 12.92% | $3.9 \cdot 10^{-2}$ | $9.3 \cdot 10^{-2}$ | 5 000 |
| | | val. | 5.84 % | 12.73 % | $4.8 \cdot 10^{-2}$ | $1.2 \cdot 10^{-1}$ | |
| | 75% | train. | 5.03% | 11.63% | $3.2 \cdot 10^{-2}$ | $7.7 \cdot 10^{-2}$ | 5 000 |
| | | val. | **5.18 %** | **11.60 %** | $4.2 \cdot 10^{-2}$ | $1.1 \cdot 10^{-1}$ | |

# Results on $\approx 5\,000$ Type II Geometries

| | training data | error | $\frac{\|u_{NN}-u\|_2}{\|u\|_2}$ | $\frac{\|p_{NN}-p\|_2}{\|p\|_2}$ | mean residual momentum | mean residual mass | # epochs trained |
|---|---|---|---|---|---|---|---|
| data-based | 10% | train. | 2.07% | 10.98% | $1.1 \cdot 10^{-1}$ | $1.4 \cdot 10^{0}$ | 500 |
| | | val. | 4.48 % | 15.20 % | $1.6 \cdot 10^{-1}$ | $1.7 \cdot 10^{0}$ | |
| | 25% | train. | 1.93% | 8.45% | $9.1 \cdot 10^{-2}$ | $1.2 \cdot 10^{0}$ | 500 |
| | | val. | 3.49 % | 10.70 % | $1.2 \cdot 10^{-1}$ | $1.4 \cdot 10^{0}$ | |
| | 50% | train. | 1.48% | 8.75% | $9.0 \cdot 10^{-2}$ | $1.1 \cdot 10^{0}$ | 500 |
| | | val. | 2.70 % | 10.09 % | $1.1 \cdot 10^{-1}$ | $1.2 \cdot 10^{0}$ | |
| | 75% | train. | 1.43% | 7.30% | $1.0 \cdot 10^{-1}$ | $1.5 \cdot 10^{0}$ | 500 |
| | | val. | **2.52 %** | **8.67 %** | $1.2 \cdot 10^{-1}$ | $1.5 \cdot 10^{0}$ | |
| physics-aware | 10% | train. | 5.35% | 12.95% | $3.5 \cdot 10^{-2}$ | $7.8 \cdot 10^{-2}$ | 5 000 |
| | | val. | 6.72% | 15.39% | $6.7 \cdot 10^{-2}$ | $2.0 \cdot 10^{-1}$ | |
| | 25% | train. | 5.03% | 12.26% | $3.2 \cdot 10^{-2}$ | $7.3 \cdot 10^{-2}$ | 5 000 |
| | | val. | 5.78 % | 13.38 % | $5.3 \cdot 10^{-2}$ | $1.4 \cdot 10^{-1}$ | |
| | 50% | train. | 5.81% | 12.92% | $3.9 \cdot 10^{-2}$ | $9.3 \cdot 10^{-2}$ | 5 000 |
| | | val. | 5.84 % | 12.73 % | $4.8 \cdot 10^{-2}$ | $1.2 \cdot 10^{-1}$ | |
| | 75% | train. | 5.03% | 11.63% | $3.2 \cdot 10^{-2}$ | $7.7 \cdot 10^{-2}$ | 5 000 |
| | | val. | **5.18 %** | **11.60 %** | $4.2 \cdot 10^{-2}$ | $1.1 \cdot 10^{-1}$ | |

$\rightarrow$ The results for the **physics-aware approach** are **comparable to the data-based approach**; the **errors are slightly higher**. However, no **reference data at all is needed for the training**.

# Generalization With Respect to the Inflow Velocity

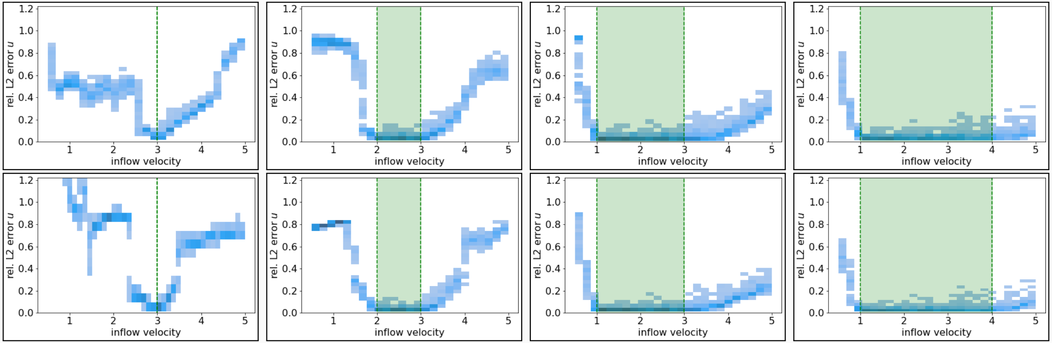


| order | # data | range inflow vel. | [0.5, 1.0] | [1.0, 2.0] | [2.0, 3.0] | [3.0, 4.0] | [4.0, 5.0] |
|---|---|---|---|---|---|---|---|
| 2 | 1 000 | [3.0, 3.0] | 55.5 % | 48.1 % | 31.1 % | 17.4 % | 61.5 % |
| | | [2.0, 3.0] | 89.3 % | 57.4 % | **4.0 %** | 15.5 % | 59.1 % |
| | | [1.0, 3.0] | 40.2 % | **3.8 %** | **4.3 %** | 7.1 % | 20.4 % |
| | | [1.0, 4.0] | 31.3 % | **4.0 %** | **4.3 %** | **5.8 %** | 7.7 % |
| 2 | 4 500 | [3.0, 3.0] | 186.8 % | 87.1 % | 40.5 % | 36.9 % | 70.6 % |
| | | [2.0, 3.0] | 78.4 % | 44.3 % | **3.2 %** | 16.1 % | 68.2 % |
| | | [1.0, 3.0] | 38.7 % | **2.9 %** | **3.4 %** | 6.7 % | 18.5 % |
| | | [1.0, 4.0] | 27.7 % | **3.1 %** | **3.4 %** | **4.7 %** | 7.2 % |

**Training:** 500 geometries **Validation:** $\approx 1\,200$ geometries

Relative $L2$-error on the validation data set in $u$: **4.9** %, in $p$: **9.5** %.

$u$: 3.3%, $p$: 7.4%

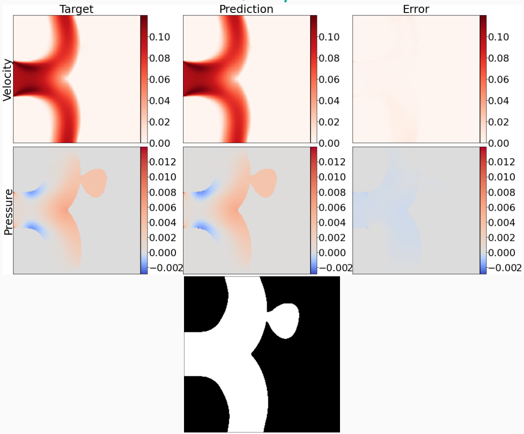


$u$: 13.2%, $p$: 35.1%

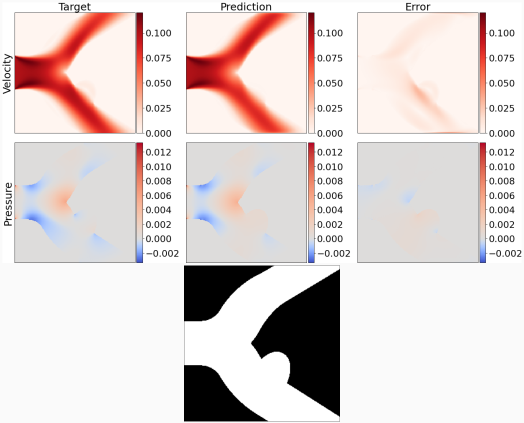

# Thank you for your attention!

## Summary

- The new field of **Scientific Machine Learning** deals with the **combination of scientific computing and machine learning** techniques; **physics-informed machine learning** models allow for the **combination of physical models and data**.
- **Domain decomposition methods** can help to **improve the training process for PINNs**, especially for (but not restricted to) **large domains** and/or **multiscale problems**.
- The **FBPINN method integrates domain decomposition approaches into PINN training** in a natural way; it can also be extended to a **two-level method**.
- Using **CNNs on image data** yields an **operator learning approach for predicting fluid flow** inside **varying computational domains**; again, the **model training can be enhanced by using physics**.


## Acknowledgements

- The **Helmholtz School for Data Science in Life, Earth and Energy (HDS-LEE)**